3D Finite-Difference Numerical Simulations in Seismic Gradiometry

David F. Aldridge, Neill P. Symons, and Matthew M. Haney

Geophysics Department, Sandia National Laboratories, Albuquerque, New Mexico

Introduction

We use the phrase ***seismic gradiometry*** to refer to the developing research area involving measurement, modeling, analysis, and interpretation of spatial derivatives (or differences) of a seismic wavefield. Analogous to gradiometric methods used in gravity and magnetic exploration, seismic gradiometry offers the potential for enhancing resolution, and revealing new (or hitherto obscure) information contained in observed seismic data. For example, measurement of pressure (proportional to div **u**) and rotation (equal to **curl u**) enables the decomposition of recorded seismic data into compressional (P) and shear (S) components.

Seismic wave propagation algorithms based on the explicit, time-domain, finite-difference (FD) numerical method are well-suited for investigating gradiometric phenomena. We have implemented in our acoustic, elastic, and poroelastic algorithms a point receiver that records the nine components of the particle velocity gradient tensor. Divergence and curl of particle displacement are obtained by forming particular linear combinations of these tensor components, and then integrating with respect to time. All algorithms emit 3D O(2,4) FD solutions of coupled, first-order systems of partial differential equations on uniformly-spaced, staggered, spatial and temporal grids. Synthetic poroelastic traces recorded by 3C geophones, hydrophones, and 3C rotation sensors in a shallow-subsurface crosswell configuration clearly indicate P and S separation of direct arrivals, as well as surface reflected and converted phases. Vertical timeslices of composite medium responses (a porosity weighted linear combination of solid and fluid responses) also show clear P and S wavefield decomposition. Interpretation of events is substantially enhanced.

Velocity-Stress-Pressure Poroelastic System and 3D FD Grid

Thirteen, coupled, first-order, non-homogeneous, partial differential equations:

$$\rho_{11}\frac{\partial \mathbf{v}_s}{\partial t} + \rho_{12}\frac{\partial \mathbf{v}_f}{\partial t} + b(\mathbf{v}_s - \mathbf{v}_f) - (1-\phi)\,\nabla\cdot\sigma_s = (1-\phi)\left(\mathbf{f}_s + \nabla\cdot\mathbf{m}_s^{asym}\right)$$

$$\rho_{12}\frac{\partial \mathbf{v}_s}{\partial t} + \rho_{22}\frac{\partial \mathbf{v}_f}{\partial t} - b(\mathbf{v}_s - \mathbf{v}_f) + \phi\,\nabla p = \phi\left(\mathbf{f}_f + \nabla\cdot\mathbf{m}_f^{asym}\right)$$

$$(1-\phi)\frac{\partial \sigma_s}{\partial t} - A\,(\nabla\cdot\mathbf{v}_s)\,\mathbf{I} - Q\,(\nabla\cdot\mathbf{v}_f)\,\mathbf{I} - \mu\left(\nabla\mathbf{v}_s + \nabla\mathbf{v}_s^T\right)\mathbf{I} = \frac{\partial \mathbf{m}_s^{sym}}{\partial t}$$

$$\phi\frac{\partial p}{\partial t} + Q\,(\nabla\cdot\mathbf{v}_s) + R\,(\nabla\cdot\mathbf{v}_f) = -\frac{\phi}{3}\frac{\partial}{\partial t}\mathrm{Tr}\{\mathbf{m}_f^{sym}\}$$

Staggered Spatial Grid

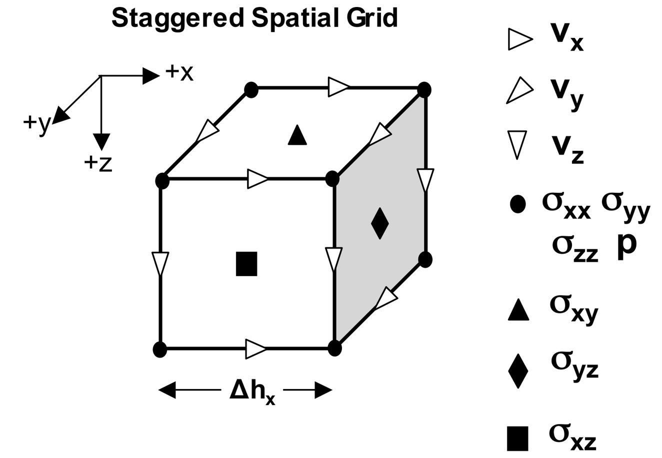

Staggered Temporal Grid

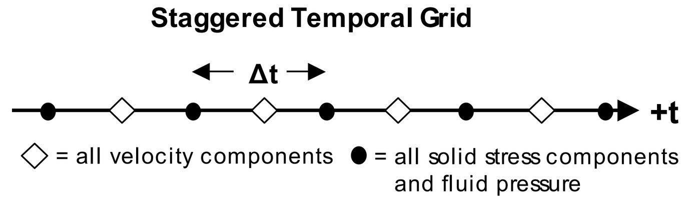

Wavefield Variables:
- $\mathbf{v}_s(\mathbf{x},t)$ – solid velocity vector
- $\mathbf{v}_f(\mathbf{x},t)$ – fluid velocity vector
- $\sigma(\mathbf{x},t)$ – solid stress tensor
- $p(\mathbf{x},t)$ – fluid pressure

Poroelastic Earth Model Parameters:
- $\phi(\mathbf{x})$ – porosity
- $\rho_{11}(\mathbf{x}), \rho_{12}(\mathbf{x}), \rho_{22}(\mathbf{x})$ – inertial coupling coefficients
- $b(\mathbf{x})$ – viscous coupling coefficient
- $A(\mathbf{x}), Q(\mathbf{x}), R(\mathbf{x})\ \mu(\mathbf{x})$ – moduli

Seismic Body Sources:
- $\mathbf{f}_s(\mathbf{x},t)$ – solid force density vector
- $\mathbf{f}_f(\mathbf{x},t)$ – fluid force density vector
- $\mathbf{m}_s(\mathbf{x},t)$ – solid moment density tensor
- $\mathbf{m}_f(\mathbf{x},t)$ – fluid moment density tensor

3D velocity-stress-pressure system is numerically solved with an explicit, time-domain, O(2,4) staggered-grid, FD algorithm

Velocity Gradient Receiver: The *Tensor Sensor*

$\frac{\partial v_x}{\partial x}, \frac{\partial v_y}{\partial y}, \frac{\partial v_z}{\partial z}$, or div $\mathbf{v}$

$\frac{\partial v_x}{\partial y}, \frac{\partial v_y}{\partial x}$, or $[\mathbf{curl\ v}]_z$

$\frac{\partial v_y}{\partial z}, \frac{\partial v_z}{\partial y}$, or $[\mathbf{curl\ v}]_x$

$\frac{\partial v_z}{\partial x}, \frac{\partial v_x}{\partial z}$, or $[\mathbf{curl\ v}]_y$

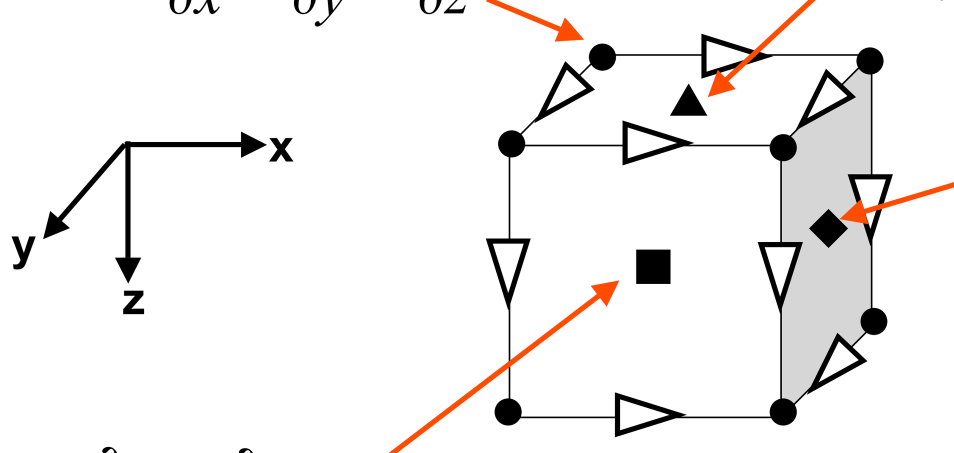

Spatial staggering implies all tensor components are approximated with centered FD operators, although all are not stored at the same location.

Shallow-Subsurface Crosswell Data Acquisition Example

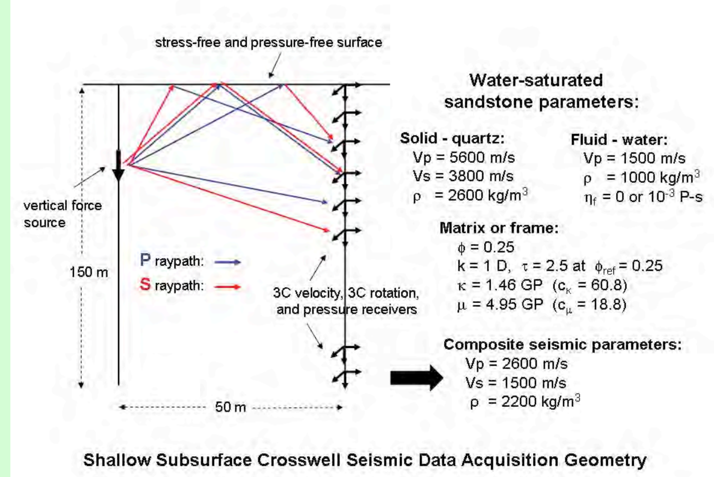

Shallow Subsurface Crosswell Seismic Data Acquisition Geometry

1) Observed events are direct (well-to-well) **P** and **S** waves, and surface-induced reflections and mode conversions.

2) y-component of velocity (Vy), and x- and z-components of rotation (Rx, Rz) vanish due to symmetry for this (homogeneous) model and recording geometry.

3) Realistic viscosity (10^{-3} P-s) of pore-saturating brine water *severely* attenuates the slow compressional wave (**Ps**).

4) Solid and fluid velocity and rotation traces are virtually identical when viscosity is nonzero.

5) Slow Ps wave has larger amplitudes in fluid velocity vs. solid velocity seismograms, and approximately same amplitude in pressure and rotation seismograms.

6) Moment density (explosion) source generates no outgoing **S** waves, as well as significantly larger amplitudes in fluid velocity and pressure, compared with force source.

7) Pressure (div) and rotation (**curl**) sensors effectively discriminate against all **S** and **P** arrivals, respectively.

8) Fluid pressure, but *not* solid pressure, vanishes on surface z = 0 due to boundary condition (solid stress vector and fluid pressure vanish).

Sandia National Laboratories is a multiprogram science and engineering facility operated by Sandia Corporation, a Lockheed-Martin Company, for the US Department of Energy under contract DE-AC04-94AL85000.

Force Source – Ideal Water

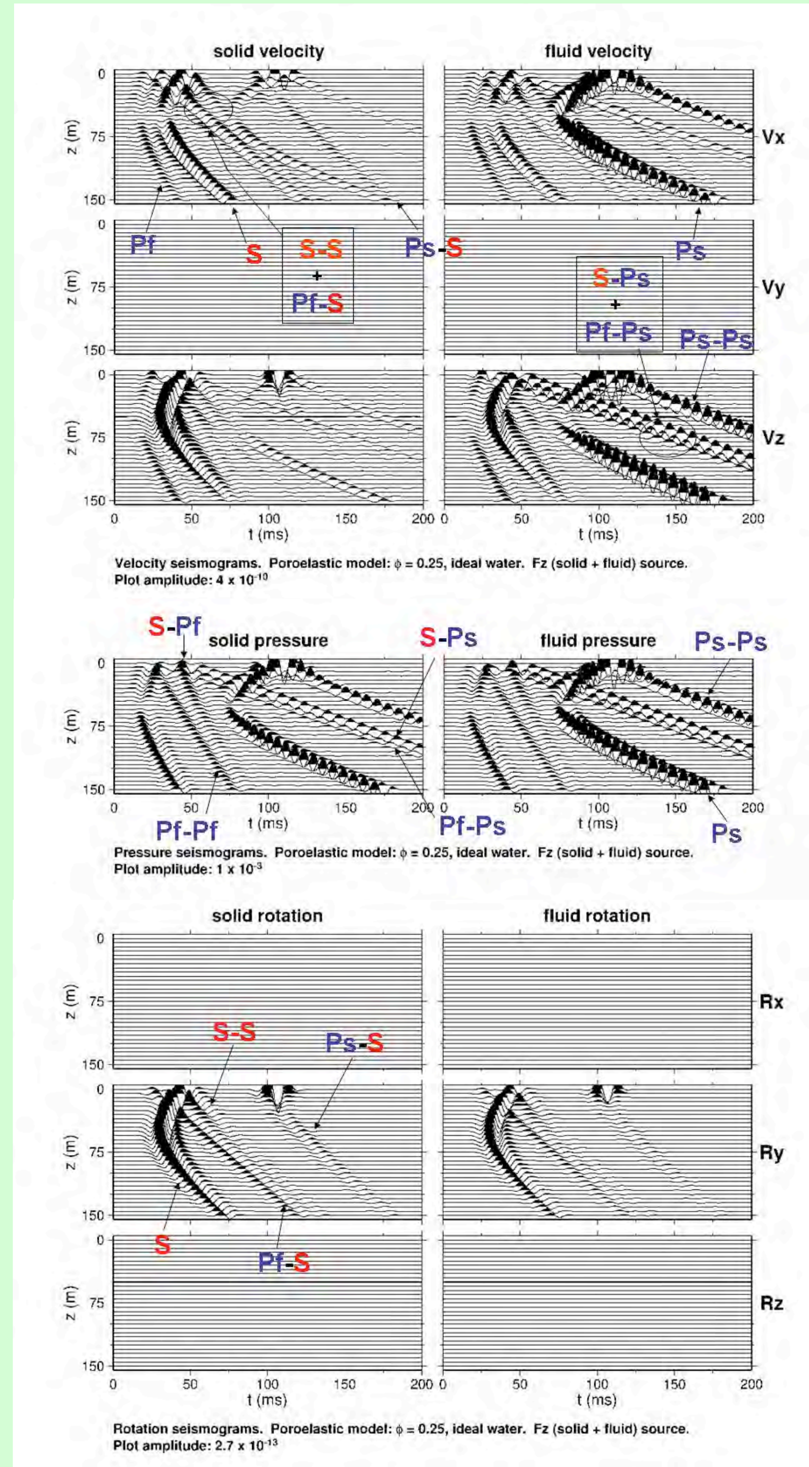

Force Source – Viscous Water

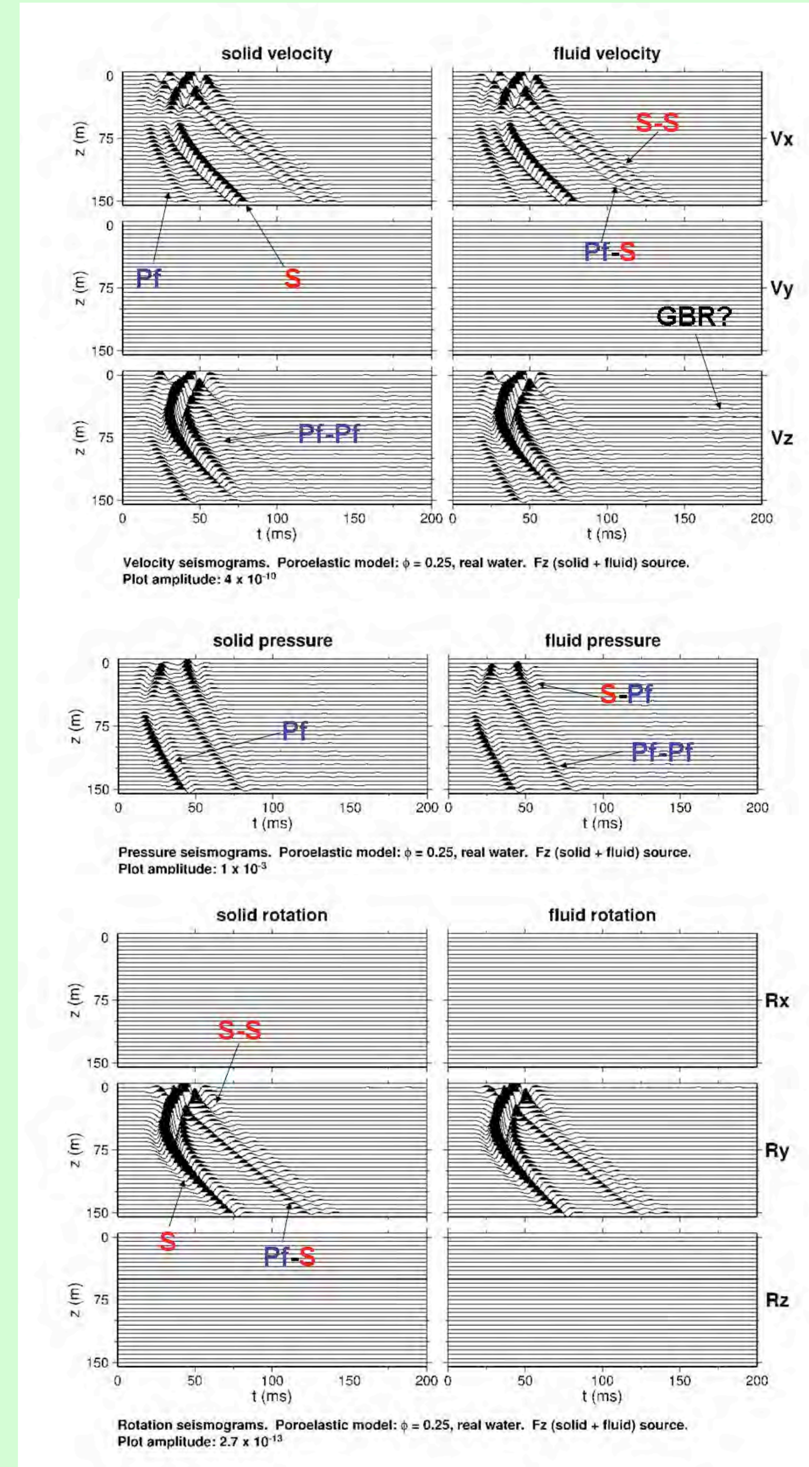

Explosion Source – Ideal Water

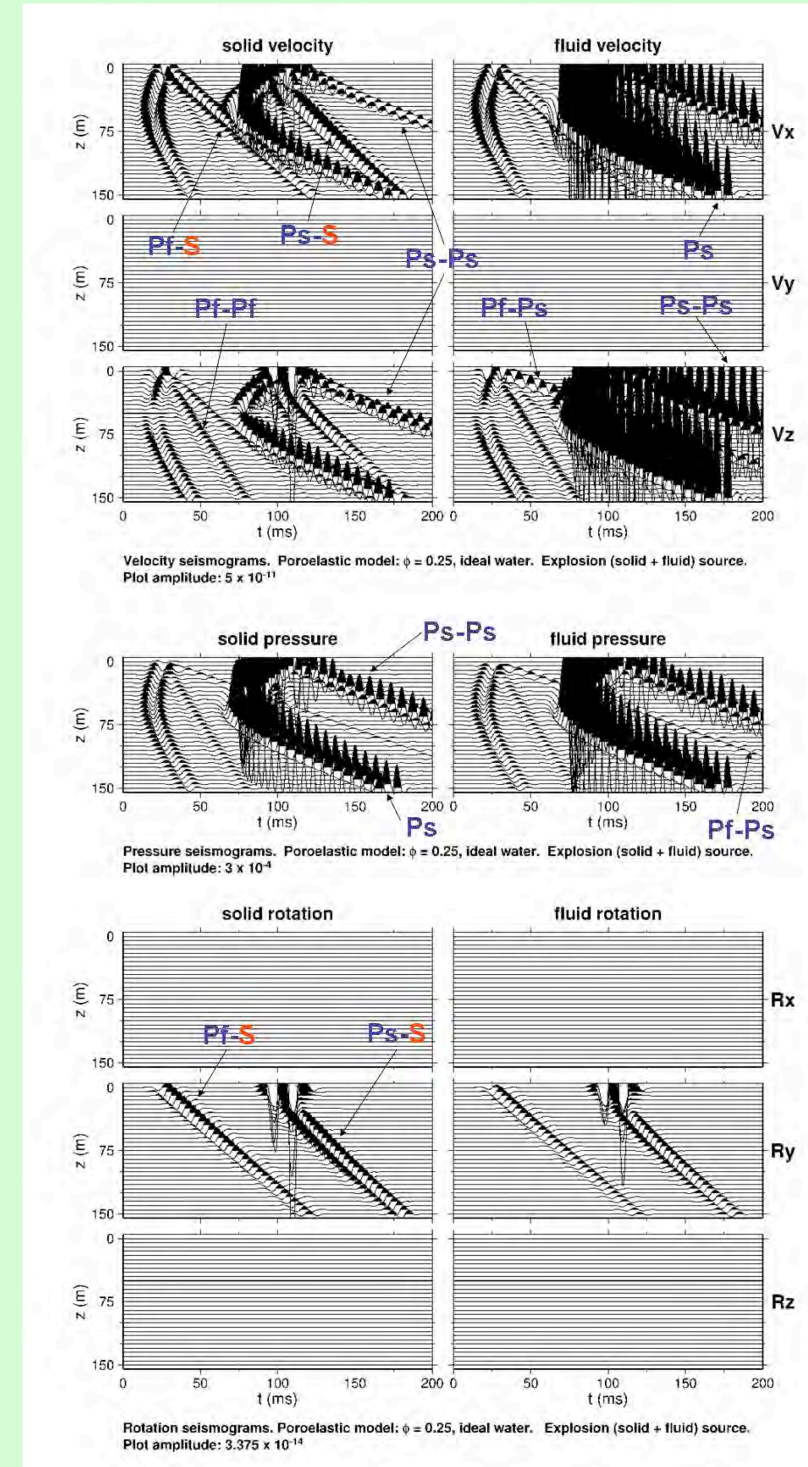

Explosion Source – Viscous Water

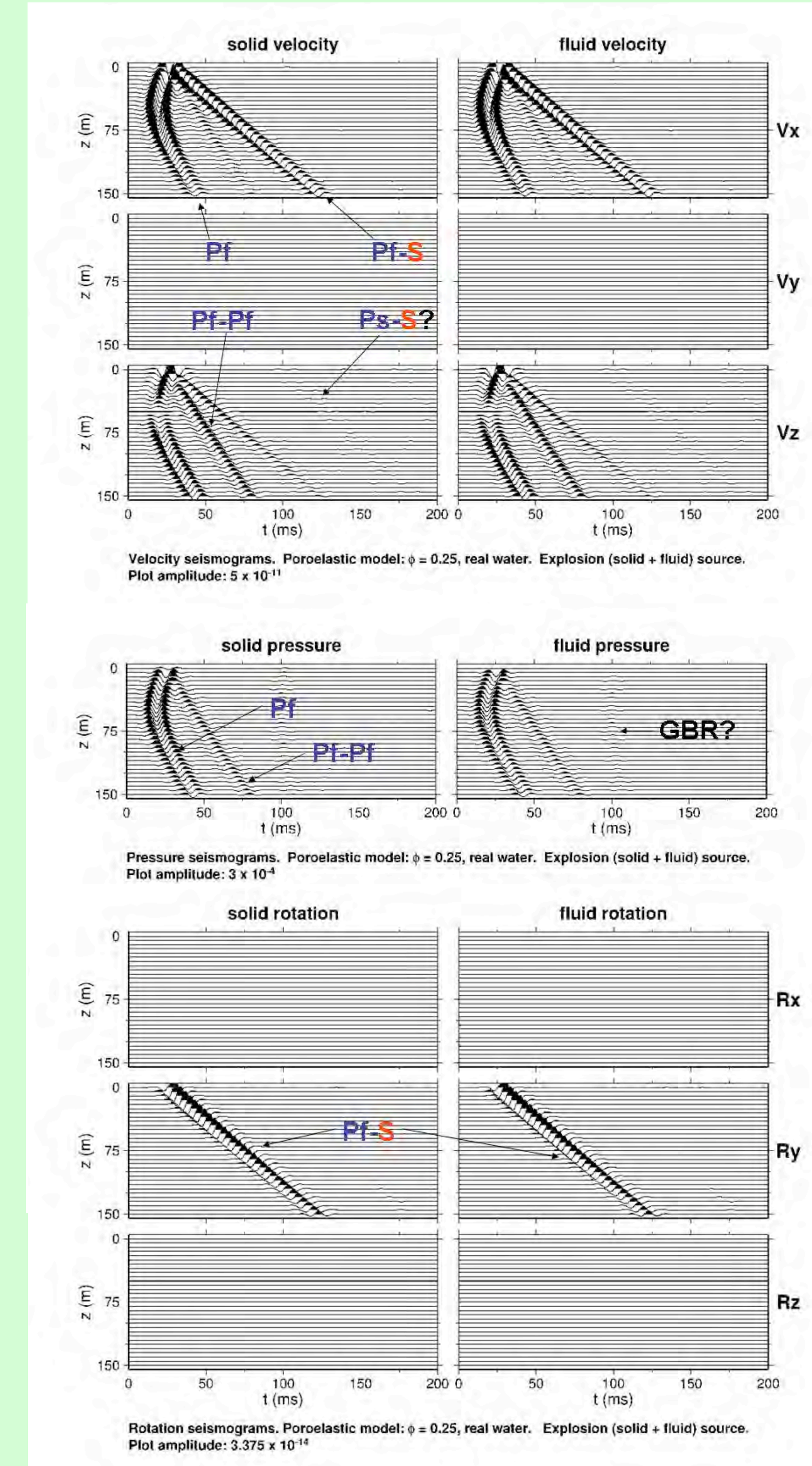

Force source

Explosion source

Composite Vz

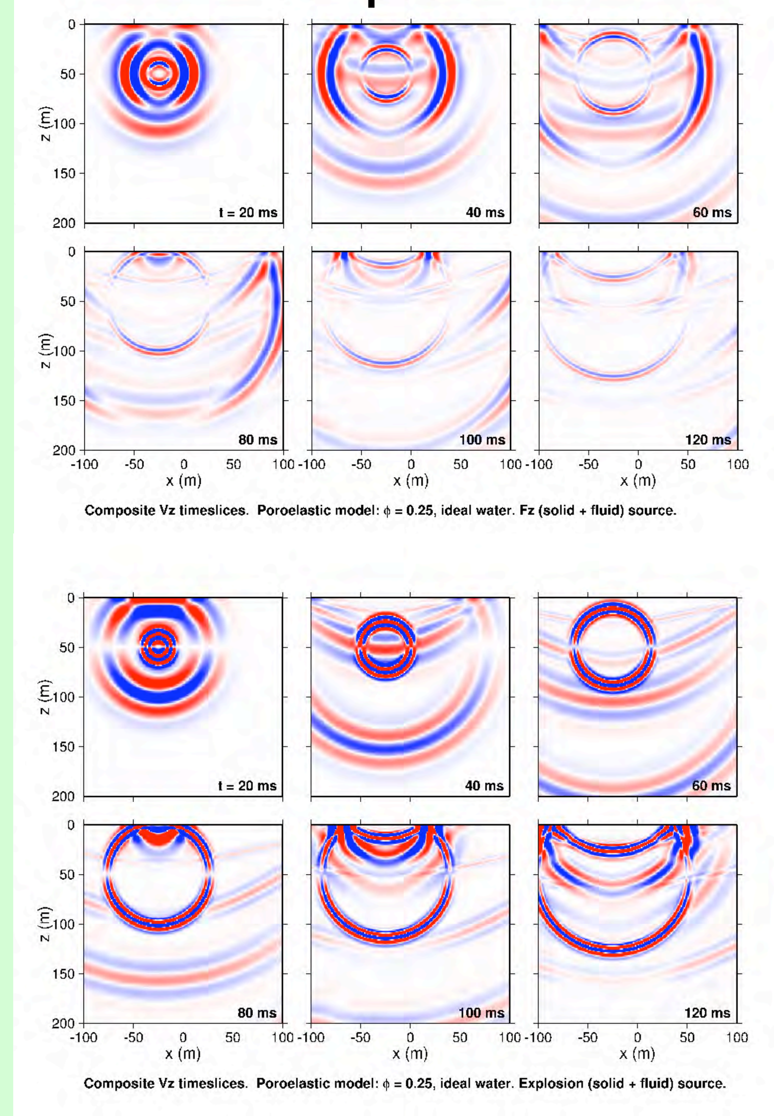

Composite P

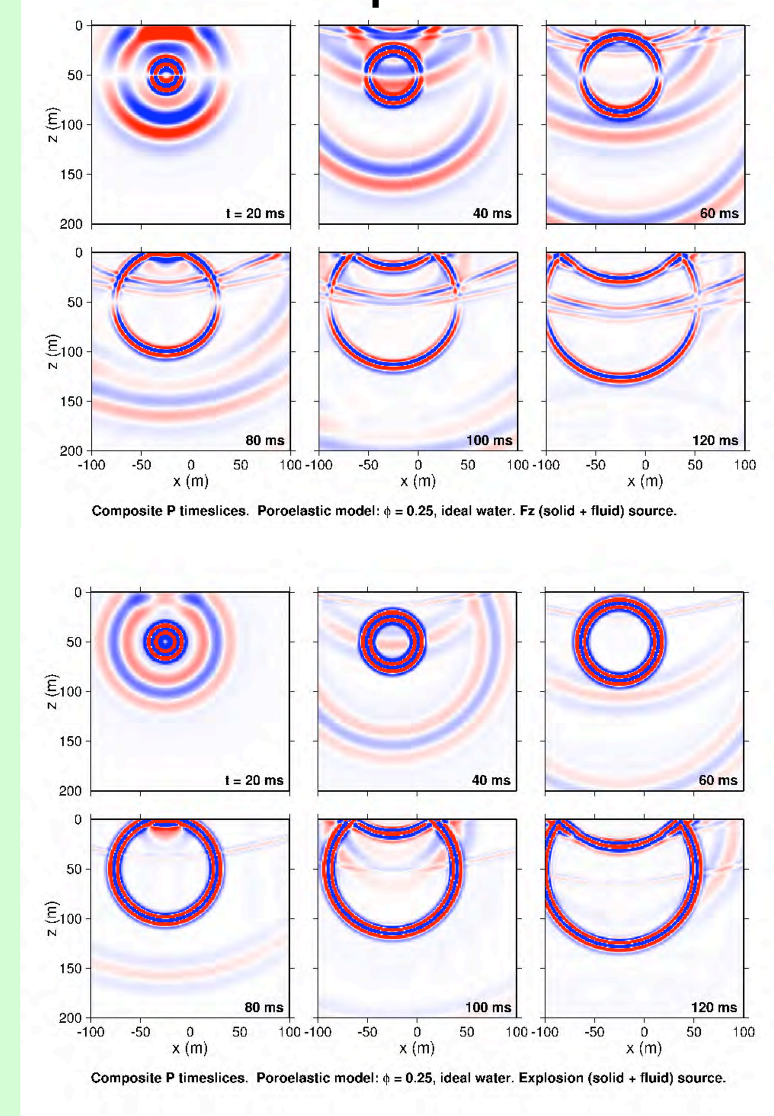

Composite dRy/dt

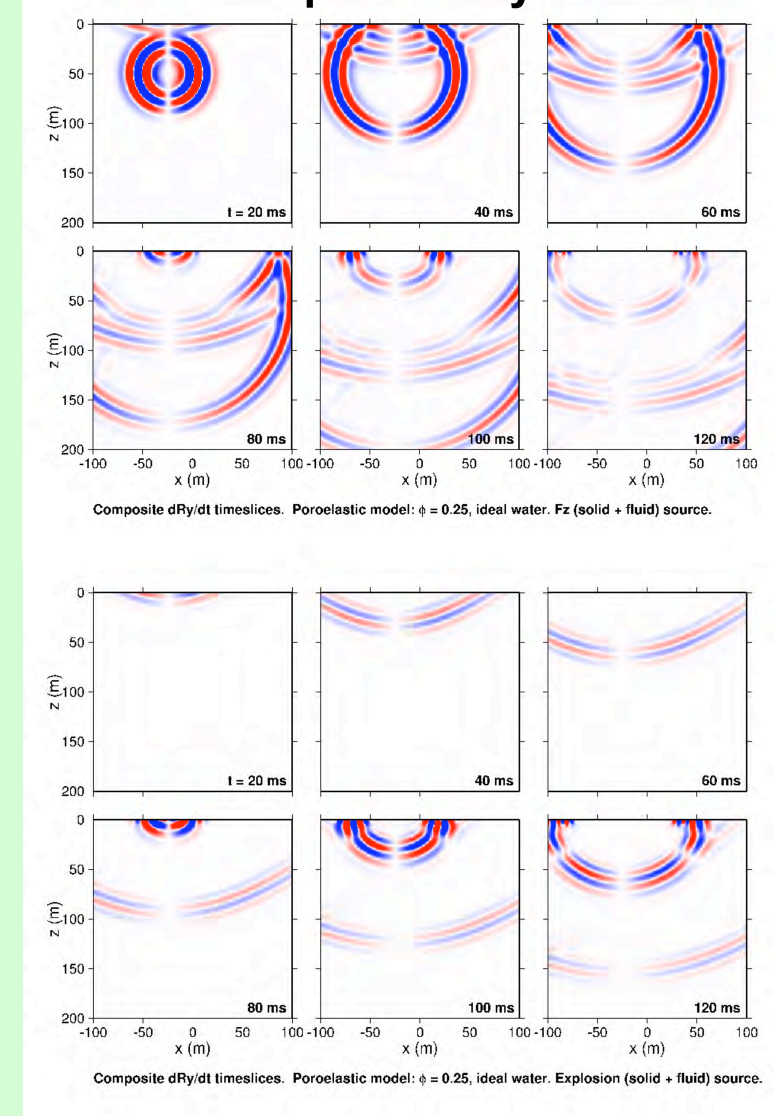

1) Timeslice displays illustrate clear separation of P and S waves:

Vz slices: both P and S wavefronts

P slices: only P wavefronts

ω_y=dRy/dt slices: only S wavefronts

2) Modeling conducted with poroelastic medium with *vanishing* fluid viscosity, in order to generate slow P wave.

3) Composite responses are porosity-weighted linear superpositions of solid and fluid responses:

$$\mathbf{v}_c(\mathbf{x},t) = [1-\phi(\mathbf{x})]\mathbf{v}_s(\mathbf{x},t) + \phi(\mathbf{x})\mathbf{v}_f(\mathbf{x},t)$$

$$p_c(\mathbf{x},t) = [1-\phi(\mathbf{x})]p_s(\mathbf{x},t) + \phi(\mathbf{x})p_f(\mathbf{x},t)$$

$$\omega_c(\mathbf{x},t) = [1-\phi(\mathbf{x})]\omega_s(\mathbf{x},t) + \phi(\mathbf{x})\omega_f(\mathbf{x},t)$$

4) Timeslice displays depict rotation rate **curl v** in contrast with **curl u** observed by rotation receivers.